Arabian Journal of Geosciences (2019) 12: 642
https://doi.org/10.1007/s12517-019-4803-4

ORIGINAL PAPER

Uniaxial compressive study on mechanical properties of rock mass considering joint spacing and connectivity rate

L. X. Xiong [1,2] · H. J. Chen [3] · T. B. Li [1] · Y. Zhang [4]

Received: 20 January 2018 / Accepted: 4 September 2019 / Published online: 18 October 2019

Abstract

To explore the effect of joint spacing and joint connectivity rate on the uniaxial compressive strength (UCS) and elastic modulus of jointed rock mass, compression tests on preset intermittent fractured specimens were performed. Test results show that the anisotropy of UCS of jointed rock mass tends to increase with joint connectivity rate. The decreasing rates of UCS and elastic modulus of jointed rock mass, when the loading direction is perpendicular to the joint plane, are higher than those when the loading direction is parallel to the joint plane with respect to joint connectivity rate and jointing index (the ratio of the length of jointed rock mass specimen to the joint spacing). The fourth-degree polynomial function proposed in this study is appropriate to analyze the nonlinear variation law of equivalent peak UCS of jointed rock mass with joint connectivity rate. The power function proposed in this study is suitable to describe the nonlinear variation law of equivalent peak UCS and equivalent elastic modulus of jointed rock mass with jointing index. However, the number of times and the number of parameters of multiple polynomial function and the number of power function need to be determined according to site-specific test results of practical project.

Keywords Jointed rock mass · Joint spacing · Joint connectivity rate · Uniaxial compression test · Peak uniaxial compressive strength · Elastic modulus

Introduction

To study the mechanical properties of jointed rock mass is challenging, as the strength and deformability of rock mass are significantly influenced by the distribution of joints. The failure modes of rock mass also vary markedly with the variation of joint orientation, spacing, and number of joints (Zhao et al. 2015). Joint spacing and joint connectivity rate are the two critical characteristics of joint geometry. At present, some researchers have carried out experimental and numerical studies on the influence of joint spacing and joint connectivity rate on the mechanical properties of jointed rock mass.

Chen et al. (2012) investigated the combined influence of joint inclination and joint continuity factor on deforming behavior of jointed rock mass for gypsum specimens with a set of non-persistent open flaws under uniaxial compression. Bahaaddini et al. (2013) conducted numerical investigation on the effect of joint geometrical parameters on the mechanical properties of a non-persistent jointed rock mass under uniaxial compression, considering joint orientation, joint spacing, joint persistency, and joint aperture. Chen et al. (2013) carried

Responsible Editor: Abdullah M. Al-Amri

✉ L. X. Xiong
xionglx1982@126.com

H. J. Chen
hjchen@nhri.cn

T. B. Li
ltb@cdut.edu.cn

Y. Zhang
zhyao@umich.edu

[1] State Key Laboratory of Geohazard Prevention and Geoenvironment Protection, Chengdu University of Technology, Chengdu 610059, Sichuan Province, China

[2] Key Laboratory of Geotechnical and Underground Engineering of Ministry of Education, Tongji University, Shanghai 200092, China

[3] Geotechnical Engineering Department, Nanjing Hydraulic Research Institute, Nanjing 210029, Jiangsu Province, China

[4] Terracon Consultants, 13050 Eastgate Park Way, Louisville, KY, USA

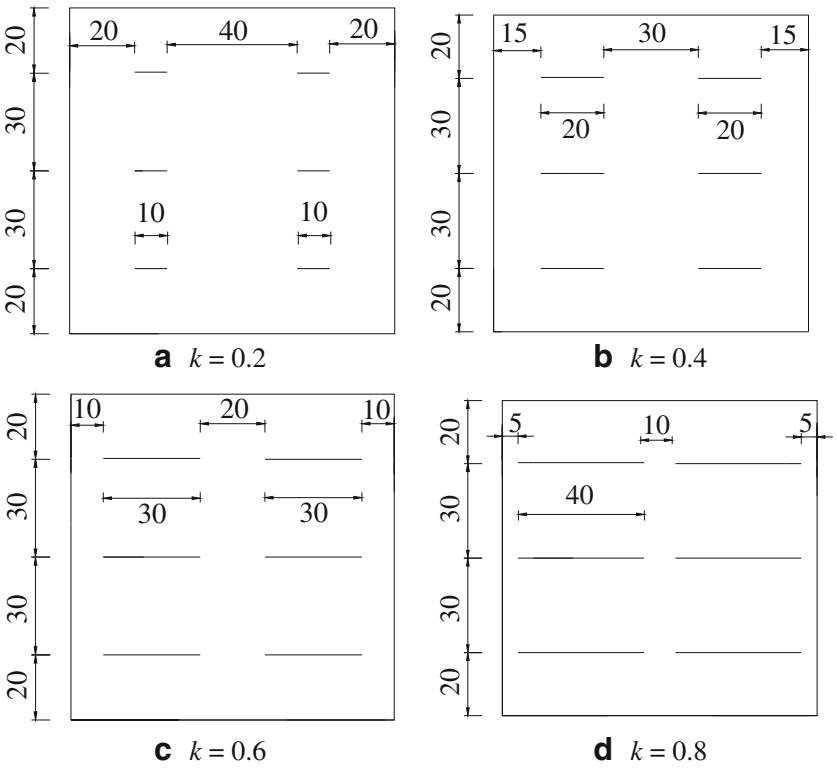

Fig. 1 Jointed rock mass specimens with different joint connectivity rates (unit: mm). k = 0.2 (**a**), k = 0.4 (**b**), k = 0.6 (**c**), k = 0.8 (**d**)

out a series of uniaxial compression tests on gypsum specimens with regularly arranged multiple parallel pre-existing joints, to study the dependence of cracking process of jointed rock mass on joint orientation and joint continuity factor. Bahaaddini et al. (2015) studied the effect of joint geometrical parameters of non-persistent rock mass on uniaxial

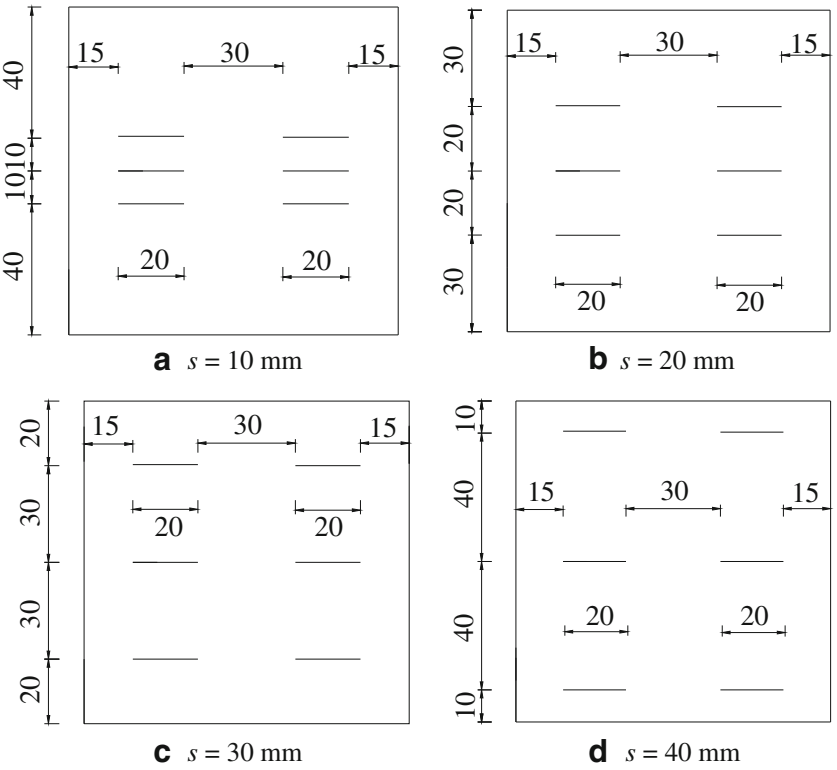

Fig. 2 Jointed rock mass specimens with different joint spacings (unit: mm). s = 10 mm (**a**), s = 20 mm (**b**), s = 30 mm (**c**), s = 40 mm (**d**)

Fig. 3 WAW-600C universal testing machine

compressive strength (UCS) and the deformation modulus using PFC^{3D}. Fan et al. (2015a, b) studied the crack initiation stress and strain of jointed rock mass containing multiple cracks under uniaxial compressive loading using PFC^{3D}, considering effects of joint inclination and joint continuity factor. Yang et al. (2016) conducted numerical simulation of rock blocks with non-persistent open joints under uniaxial compression using the particle flow modeling method. Liu et al. (2017) experimentally investigated the influences of joint dip angle, joint persistency, joint density, and joint spacing on the fatigue of synthetic jointed rock models. Yang et al. (2017) carried out a physical experiment to better understand the mechanical behavior of jointed rock mass, considering the effects of joint interaction, joint spacing, and joint dip angle. Chen et al. (2018) numerically studied the effect of joint strength mobilization on the mechanical behavior of jointed rock mass using PFC^{2D}. Yang and Qiao (2018) investigated the shear behavior and failure mechanism of granite material bridges between discontinuous joints subjected to direct shearing using a flat-joint modeling approach.

The above scholars only studied the variation of mechanical properties of specimens containing non-persistent joints with the geometric parameters of the joints by conducting experiments or numerical simulations. Few scholars have proposed corresponding formulas to analyze the variation of compressive strength of jointed rock mass with joint spacing and joint connectivity rate.

In this study, various compression tests on preset intermittent fractured specimens were performed, in order to understand the effects of joint spacing and joint connectivity rate on the strength and deformation of jointed rock mass systematically. The fitting formulas for the variations of the UCS and elastic modulus of jointed rock mass with joint spacing and connectivity rate are proposed.

Experimental setup

Specimen size and arrangement of joints

The specimens used in this study have dimensions of 10 cm × 10 cm × 10 cm. Non-persistent joints were created by inserting planks with thickness of 1 mm into a mold after setting the material. The jointed rock mass specimen with joint connectivity rates of 0, 0.2, 0.4, 0.6, and 0.8 was prepared. The joint spacing is maintained at 30 mm, as shown in Fig. 1.

The jointed rock mass specimen with joint spacings of 10 mm, 20 mm, 30 mm, and 40 mm and connectivity rate of 0.4 is shown in Fig. 2.

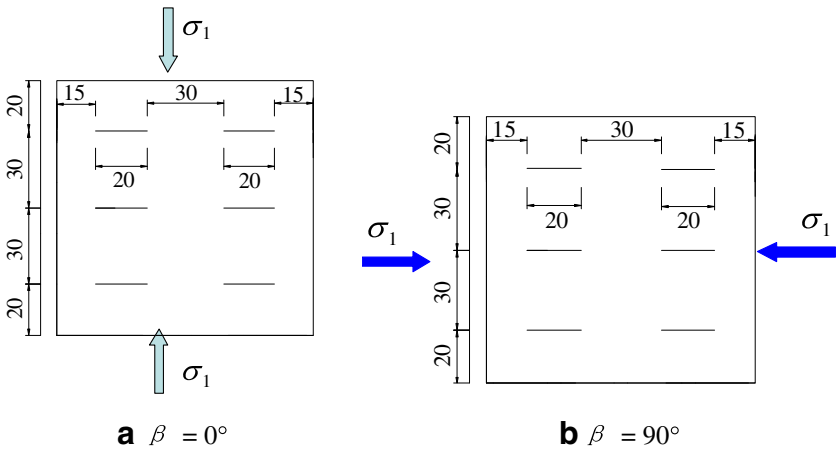

Fig. 4 The relationship between the loading direction and the joint plane. $\beta = 0°$ (**a**), $\beta = 90°$ (**b**)

Table 1 Experimental groups of uniaxial compression tests

No.	Joint spacing/mm	Joint connectivity rate	Geometric relationship between the loading direction and the joint plane
L-0-T	0	0	Perpendicular
L-0-P	0	0	Parallel
L-10-T	30	0.2	Perpendicular
L-10-P	30	0.2	Parallel
L-20-T	30	0.4	Perpendicular
L-20-P	30	0.4	Parallel
L-30-T	30	0.6	Perpendicular
L-30-P	30	0.6	Parallel
L-40-T	30	0.8	Perpendicular
L-40-P	30	0.8	Parallel
S-10-T	10	0.4	Perpendicular
S-10-P	10	0.4	Parallel
S-20-T	20	0.4	Perpendicular
S-20-P	20	0.4	Parallel
S-40-T	40	0.4	Perpendicular
S-40-P	40	0.4	Parallel

Preparation of model materials and specimens

Specimens were cast by pouring cement mortar with water/cement ratio of 0.65 into the mold. Cement No. 425 used in this study was produced by the China Building Materials Academy. The ISO standard sand was used which is conformed to Chinese National Standard GB/T17671-1999. Its particle size ranges from 0.5 to 1.0 mm.

After the initial setting of the cement mortar, wood plank was inserted into position as marked by the short-line shown in Figs. 1 and 2. The length of the wood planks is 10 cm, and the wood planks remained permanently in the specimens.

Test machine

Uniaxial compression tests were conducted using WAW-600C universal testing machine. The maximum displacement loading rate of the testing machine is 60 mm/min, and the maximum compression load is 600 kN. A picture of the testing machine is shown in Fig. 3.

In this study, the uniaxial compression tests were performed under displacement loading rate of 0.6 mm/min, approximately to a strain rate of 10^{-4} s^{-1}.

Test groups

When conducting compression test on each jointed rock mass specimen, the loading was applied in a direction that was

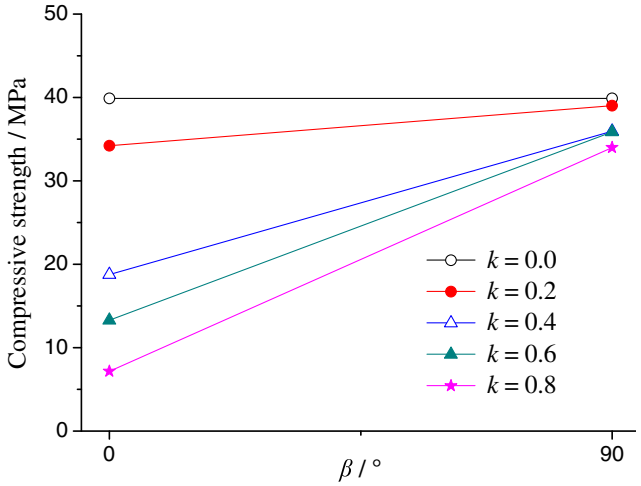

Fig. 5 The peak uniaxial compressive strengths of jointed rock mass specimen with different joint connectivity rates, k

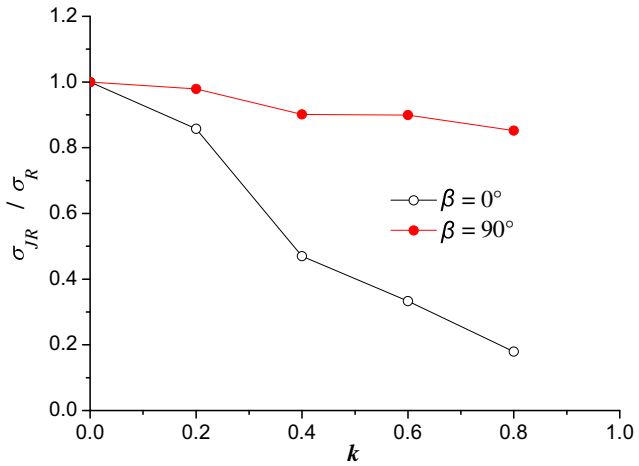

Fig. 6 Variation curves of equivalent peak UCS of jointed rock mass with joint connectivity rate when β are 90° and 0°

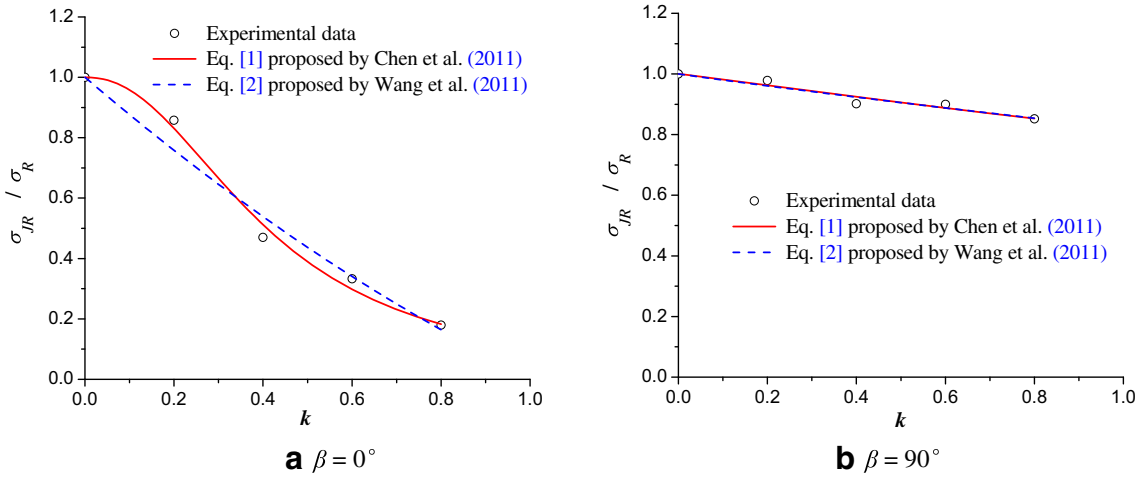

Fig. 7 The contrast result between Eq. (1) proposed by Chen et al. (2011) and Eq. (2) proposed by Wang et al. (2011). $\beta = 0°$ (**a**), $\beta = 90°$ (**b**)

either parallel or perpendicular the joint plane, as shown in Figs. 1 and 2. As for the jointed rock mass specimen with the joint connectivity rate of 0.4 and the joint spacing of 30 mm, the loading direction was set either perpendicular or parallel to the joint plane as shown in Fig. 4. Angle β of joint plane is considered as 0° when the loading direction is perpendicular to the joint plane and 90° when the loading direction is parallel to the joint plane.

The uniaxial compression tests were divided into several groups as shown in Table 1. The uniaxial compression tests were classified according to three factors, i.e., the joint connectivity rate, the joint spacing, and the geometric relationship between the loading orientation and the joint plane.

Test results of jointed rock mass with varied joint connectivity rates

Peak UCS of jointed rock mass

The comparison of UCS of jointed rock mass specimen with various joint connectivity rates, k, when the loading direction is perpendicular or parallel to the joint plane, is shown in Fig. 5.

Test results show that the peak uniaxial compressive strengths of jointed rock mass specimen with joint connectivity rates of 0, 0.2, 0.4, 0.6, and 0.8, when the loading direction is parallel to the joint plane, are greater than that when the loading direction is perpendicular to the joint plane. This coincides with the conclusions obtained by Bahaaddini et al. (2013), Fan et al. (2015a, b), Bahaaddini et al. (2016), Yang et al. (2016), Yang et al. (2017), and Chen et al. (2018).

When the joint dip angle is low (e.g., $\beta = 0°$ and 15°), with the axial compression increasing, wing cracks developed from the pre-existing joint tips. The wing cracks are tensile cracks that initiated at an angle from the joint tips and propagated in the direction of maximum compression, and macro failure planes going through the entire specimens fail the jointed rock mass with the development of wing cracks (Yang et al. 2017). When the joint dip angle is 90°, although cracks occurred to the rock bridges between pre-existing joints and the joint plane, the joint plane has negligible effect on the failure behavior of the jointed rock mass, and this failure model can be defined as intact material failure mode (Yang et al. 2017). Therefore, the peak uniaxial compressive strength of jointed rock mass specimen with preset non-persistent joints when the loading direction is parallel to the joint plane is higher than that when the loading direction is perpendicular to the joint plane.

The difference of peak UCS of jointed rock mass specimen between when β is 90° and 0° increases with joint connectivity rate. Therefore, the anisotropy of UCS of jointed rock mass tends to increase with joint connectivity rate. The equivalent peak uniaxial compressive strengths of jointed rock mass specimen with different joint connectivity rates are shown in Fig. 6. In this figure, σ_{JR} and σ_R are the peak uniaxial

Table 2 Fitting parameters of Eq. (1) proposed by Chen et al. (2011)

β/°	p	q	R^2	Q
0	7.34464	2.22886	0.99245	0.00122
90	0.21925	1.08059	0.93865	0.00031

Table 3 Fitting parameters of Eq. (2) proposed by Wang et al. (2011)

β/°	a	b	R^2	Q
0	0.27054	− 1.26129	0.9695	0.00495
90	0.02193	− 0.19978	0.9374	0.00031

compressive strengths of jointed rock mass specimen with and without joints, respectively.

In Fig. 6, it can be noted that the peak UCS of jointed rock mass model decreases rapidly with joint connectivity rate when the loading direction is perpendicular to the joint plane. The relationship curve between the equivalent peak UCS and the joint connectivity rate is approximately linear when the loading direction is parallel to the joint plane. Therefore, the effect of joint connectivity rate on the peak UCS, when the loading direction is parallel to the joint plane, is relatively less than that on when the loading direction is perpendicular to the joint plane.

Chen et al. (2011) suggested that the nonlinear variation law of equivalent peak UCS of jointed rock mass with joint connectivity rate could be analyzed by the reciprocal expression of power function:

$$\sigma_{JR}/\sigma_R = 1/(1 + pk^q) \tag{1}$$

where p and q are the fitting parameters.

Wang et al. (2011) suggested that the nonlinear variation law of equivalent peak UCS of jointed rock mass with joint connectivity rate could be analyzed by quadratic polynomial function:

$$\sigma_{JR}/\sigma_R = ak^2 + bk + 1 \tag{2}$$

where a and b are the fitting parameters.

Equations (1) and (2) are firstly implemented into Origin software. Then, the values of the parameters of Eqs. (1) and (2) are obtained by using the nonlinear least square method. The same procedures were utilized in this paper for all subsequent formulas.

The test results shown in Fig. 6 were analyzed by using Eqs. (1) and (2), respectively. Figure 7 shows the results of Eq. (1) proposed by Chen et al. (2011) in comparison with Eq. (2) proposed by Wang et al. (2011). The square of the correlation coefficient (R^2) and the sum of least error square (Q) are chosen as discrimination criteria (Yang and Cheng 2011). The back-analyzed parameters of fitting curves between the equivalent peak UCS and joint connectivity rate, and the coefficients of R^2 and the coefficients of Q are listed in Tables 2 and 3.

The model agrees well with the experimental result when R^2 tends to 1 and Q approaches zero. Therefore, the fitting accuracy of Eq. (1) proposed by Chen et al. (2011) is higher than that of Eq. (2) proposed by Wang et al. (2011) in fitting the test data when the loading direction is perpendicular to the joint plane. The fitting accuracy of Eq. (1) proposed by Chen et al. (2011) is close to that of Eq. (2) proposed by Wang et al. (2011) in fitting the test data when the loading direction is parallel to the joint plane.

Table 4 The coefficients of R^2 using Eqs. (2)–(7) fitting

β/°	Eq. (2)	Eq. (3)	Eq. (4)	Eq. (5)	Eq. (6)	Eq. (7)
0	0.9695	0.9942	0.9827	0.9953	1.0	1.0
90	0.9374	0.9374	0.9388	0.9402	1.0	1.0

Equation (1) is the reciprocal expression of power function of joint connectivity rate, and the fitting accuracy of Eq. (1) is higher than that of Eq. (2). Therefore, the fitting accuracy of the reciprocal expression of Eq. (2) may be higher than that of Eq. (2). And the fitting accuracy of cubic polynomial function may also be higher than that of Eq. (2). These need further investigation to confirm.

Because of this, we used various functions to analyze the nonlinear variation law of equivalent peak UCS of jointed rock mass with joint connectivity rate. In this study, the quadratic polynomial function, the cubic polynomial function, and the fourth-degree polynomial function, in association with the reciprocal expression of the quadratic polynomial function, the reciprocal expression of the cubic polynomial function, and the reciprocal expression of the fourth-degree polynomial function were employed subsequently.

The reciprocal expression of the quadratic polynomial function is

$$\sigma_{JR}/\sigma_R = 1/\left(ak^2 + bk + 1\right) \tag{3}$$

The cubic polynomial function is

$$\sigma_{JR}/\sigma_R = ak^3 + bk^2 + ck + 1 \tag{4}$$

The reciprocal expression of the cubic polynomial function is

$$\sigma_{JR}/\sigma_R = 1/\left(ak^3 + bk^2 + ck + 1\right) \tag{5}$$

The fourth-degree polynomial function is

$$\sigma_{JR}/\sigma_R = ak^4 + bk^3 + ck^2 + dk + 1 \tag{6}$$

Table 5 The coefficients of Q using Eqs. (2)–(7) fitting

β/°	Eq. (2)	Eq. (3)	Eq. (4)	Eq. (5)	Eq. (6)	Eq. (7)
0	0.00495	0.00095	0.00421	0.00113	1.2942E−31	3.0815E−33
90	0.00031	0.00031	0.00046	0.00045	6.163E−32	7.3956E−32

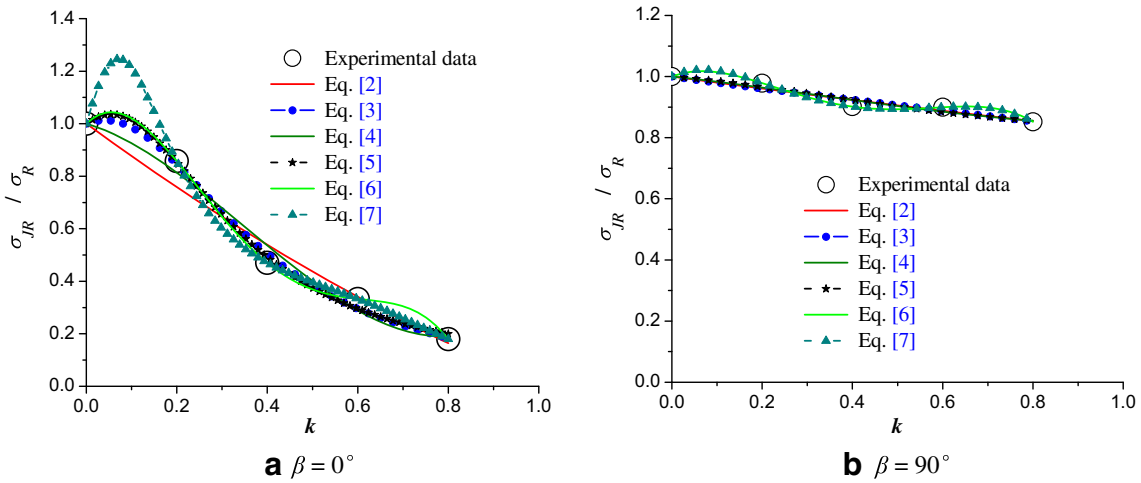

Fig. 8 The fitting curves of Eqs. (2)–(7). $\beta = 0°$ (**a**), $\beta = 90°$ (**b**)

The reciprocal expression of the fourth-degree polynomial function is

$$\sigma_{JR}/\sigma_R = 1/\left(ak^4 + bk^3 + ck^2 + dk + 1\right) \tag{7}$$

The R^2 and Q of Eqs. (2)–(7) when fitting the test data shown in Fig. 6 are given in Tables 4 and 5.

The fitting accuracy of multiple polynomial function can be significantly improved by increasing the number of times and the number of parameters of multiple polynomial functions when fitting the test data shown in Fig. 6. The R^2 obtained by the fourth-degree polynomial function is 1.0. For the quadratic polynomial function or the cubic polynomial function, R^2 will be improved and Q will be reduced when using its reciprocal expression fitting. The fitting accuracy of Eq. (6) or (7) seems to be high. The fitting curves of the test results using Eqs. (2)–(7) are shown in Fig. 8.

Although the fitting accuracy of Eq. (6) or (7) is almost identical, the fitting curve of Eq. (6) is closer to the test data, and the fitting curve of Eq. (7) is a little deviated from the test data when k is in the range of 0 to 0.2, when β is 0°. Therefore, it is preferable to use Eq. (6) for analysis. When using Eq. (6), we have:

1. When β is 0°, the relation can be expressed by

$$\sigma_{JR}/\sigma_R = -19.84365k^4 + 34.13722k^3 - 17.99275k^2 + 1.6806k + 1 \tag{8}$$

2. When β is 90°, the relation can be expressed by

$$\sigma_{JR}/\sigma_R = -6.5546k^4 + 10.59291k^3 - 5.21746k^2 + 0.56555k + 1 \tag{9}$$

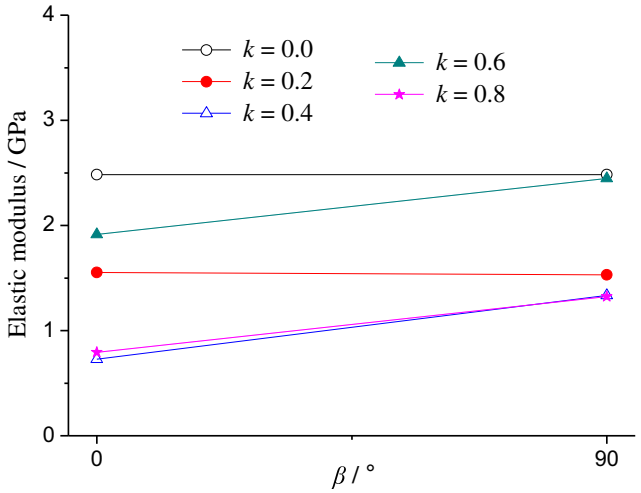

Fig. 9 The elastic modulus of jointed rock mass specimen with different joint connectivity rates

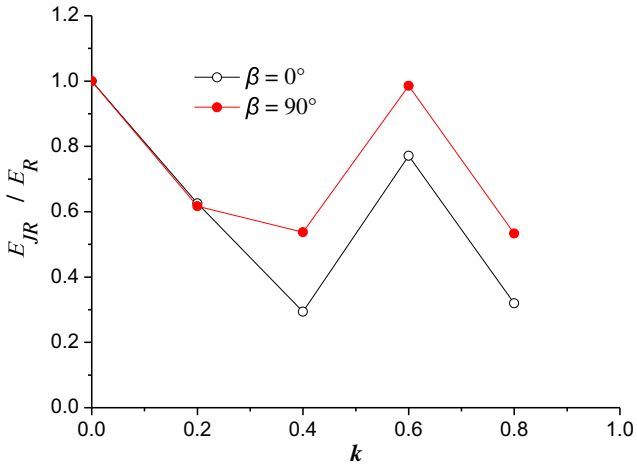

Fig. 10 Variation curves of equivalent elastic modulus with joint connectivity rate of jointed rock mass when β are 90° and 0°

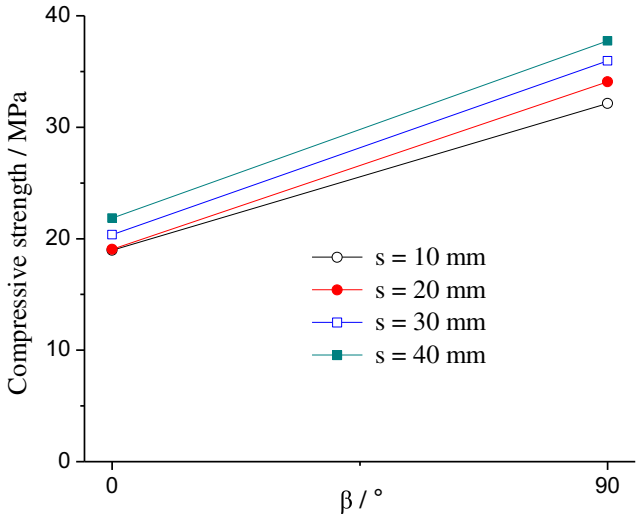

Fig. 11 The peak uniaxial compressive strengths of jointed rock mass specimen with different joint spacings

The fitting accuracy of Eq. (1) is higher than that of Eq. (2) when fitting the nonlinear variation law of equivalent peak UCS of jointed rock mass with joint connectivity rates in this study, whilst the fitting accuracy of the fourth-degree polynomial function is higher than that of Eq. (1).

Therefore, the multiple polynomial function is appropriate to analyze the nonlinear variation law of equivalent peak UCS of jointed rock mass with joint connectivity rate. The fitting accuracy of multiple polynomial function can be improved by increasing the number of times and the number of parameters, whilst the number of times and the number of parameters of multiple polynomial function need to be determined according to the lab and field test results of practical project.

Elastic modulus

The elastic modulus is calculated as a secant modulus from the origin to a defined point on the uniaxial compressive stress-strain curve, within 30% of the specimen's peak UCS. The comparison of elastic modulus of jointed rock mass model with different joint connectivity rates, when the loading direction is perpendicular and parallel to the joint plane, is shown in Fig. 9. Variation curves of equivalent elastic modulus with joint connectivity rate of jointed rock mass specimen are shown in Fig. 10. In Fig. 10, E_{JR} and E_R are elastic moduli of jointed rock mass models with and without joint, respectively.

The elastic modulus of jointed rock mass specimen decreases substantially with joint connectivity rate when the loading direction is perpendicular to the joint plane. The decreasing rate of equivalent elastic modulus of jointed rock mass specimen with joint connectivity rate when the loading direction is perpendicular to the joint plane is higher than that when the loading direction is parallel to the joint plane.

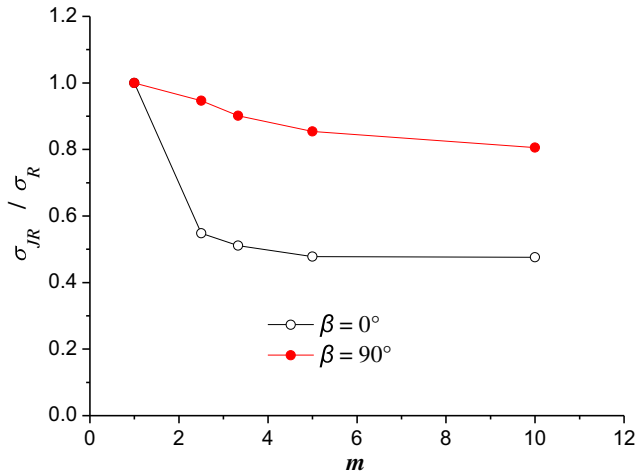

Fig. 12 Variation curves of equivalent peak uniaxial compressive strengths of jointed rock mass with jointing index

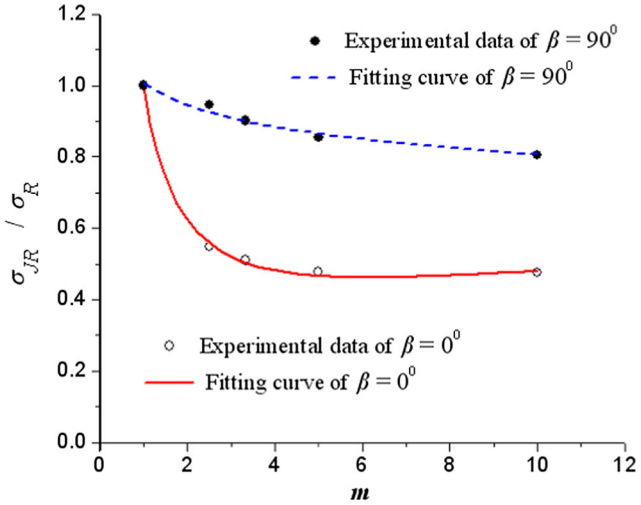

Fig. 13 Fitting curves of power function proposed in this study when analyzing the equivalent peak UCS with jointing index

Test results of jointed rock mass with varied joint spacing

Peak UCS of jointed rock mass model

The uniaxial compressive strength of jointed rock mass specimen with different joint spacings, when the loading direction

Table 6 Parameters of power function proposed in this study when analyzing the equivalent peak UCS with jointing index

β/ °	a	b	c	R^2	Q
0	− 1.00092	− 0.13421	0.92081	0.99837	0.00016
90	− 0.99082	0.04632	0.04632	0.97252	0.00032

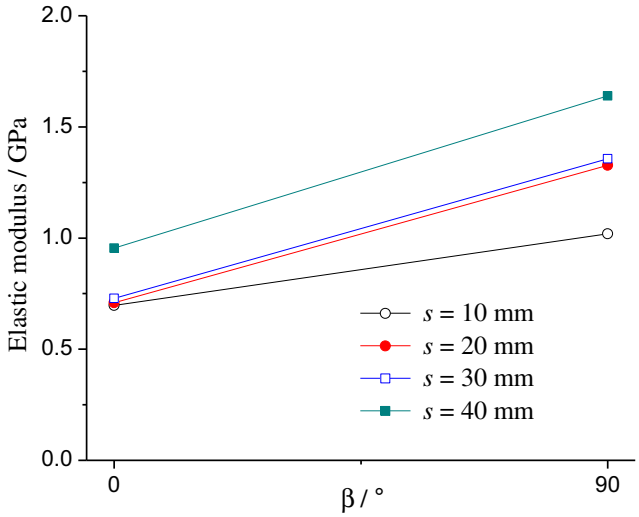

Fig. 14 The elastic moduli of jointed rock mass specimen with different joint spacings

is perpendicular or parallel to the joint plane, is shown in Fig. 11.

In Fig. 11, it is clear that the peak uniaxial compressive strength of jointed rock mass model with joint spacings of 10 mm, 20 mm, 30 mm, and 40 mm, when the loading direction is parallel to the joint plane, is greater than those when the loading direction is perpendicular to the joint plane. The peak uniaxial compressive strengths of jointed rock mass models when β is 90° and 0° both increase with joint spacing.

The jointing index m is defined as the ratio of the length of jointed rock mass specimen to the joint spacing (Chen et al. 2014):

$$m = L/s \tag{10}$$

where L is the length of jointed rock mass model, and s is the joint spacing.

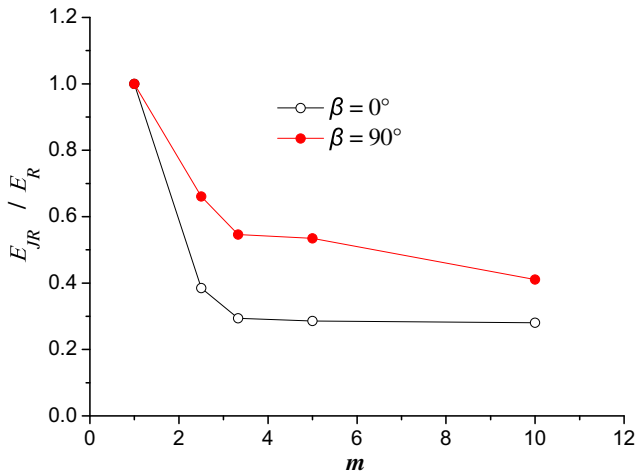

Fig. 15 Variation curves of equivalent elastic modulus with jointing index

In Eq. (10), it is known that the jointing index m is inversely proportional to the joint spacing. The denser the joint, the smaller the joint spacing and the greater the jointing index m is. The length of jointed rock mass specimen of 100 mm is adopted in this study; thus, the jointing indexes of jointed rock mass specimen with joint spacings of 100 mm, 40 mm, 30 mm, 20 mm, and 10 mm are calculated as 1.0, 2.5, 3.33, 5, and 10, respectively. Variation curves of equivalent peak uniaxial compressive strengths of jointed rock mass with jointing index, m, are shown in Fig. 12.

The peak UCS of jointed rock mass specimen decreases drastically with jointing index when the loading direction is perpendicular to the joint plane. The decreasing rate of the peak UCS of jointed rock mass specimen when the loading direction is parallel to the joint plane is relatively smaller than that when the loading direction is perpendicular to the joint plane with jointing index.

Chen et al. (2014) suggested that the nonlinear variation law of equivalent peak UCS of jointed rock mass with jointing index can be analyzed using the power function proposed by Goldstein et al. (1966):

$$\sigma_{JR}/\sigma_R = a + (1-a)m^{-b} \tag{11}$$

where a and b are the fitting parameters; m is the jointing index.

Although the fitting curve of Eq. (11) agrees well with the test data when β is 0° as shown in Fig. 10, it cannot converge when β is 90° as shown in Fig. 10. For this, we proposed a power function to analyze the test data:

$$\sigma_{JR}/\sigma_R = a + m^{-b} + m^{-c} \tag{12}$$

where a, b and c are the fitting parameters; m is the jointing index.

The fitting results are shown in Fig. 13, and the fitting parameters are listed in Table 6.

Both the fitting curves of power function proposed in this study agree well with the test data when β are 0° and 90° as shown in Fig. 10. Thus, Eq. (12) is more suitable to analyze the variation curve of equivalent peak UCS of jointed rock mass with jointing index.

Elastic modulus

The elastic moduli of jointed rock mass specimen with different joint spacings, when the loading direction is perpendicular and parallel to the joint plane, are shown in Fig. 14.

The elastic moduli of jointed rock mass specimen with joint spacings of 10 mm, 20 mm, 30 mm, and 40 mm when the loading direction is parallel to joint plane are greater than

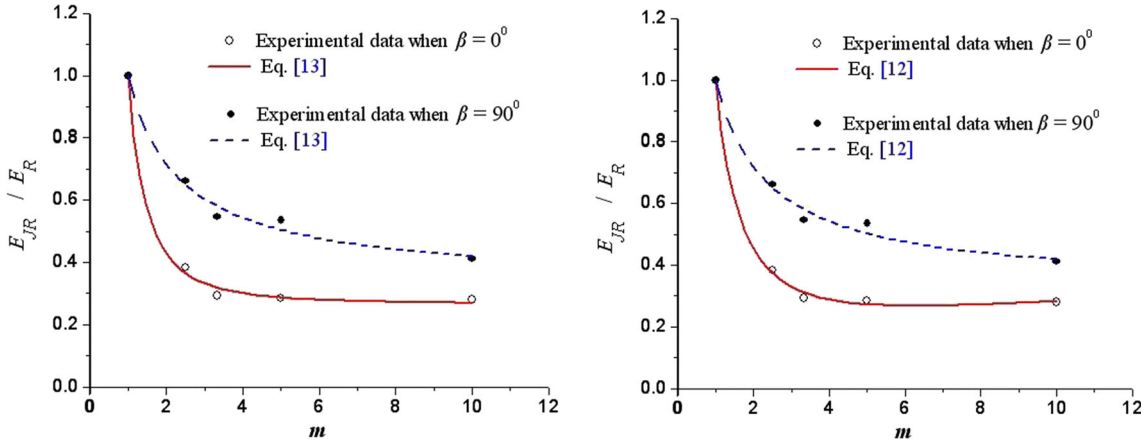

a Eq. (13) proposed by Chen et al. (2014) **b** Eq. (12) proposed in this study

Fig. 16 The fitting results using Eqs. (12) and (13) when analyzing the variation curve of equivalent elastic modulus with jointing index. Eq. (13) proposed by Chen et al. (2014) (**a**), Eq. (12) proposed in this study (**b**)

those when the loading direction is perpendicular to joint plane. The elastic moduli of jointed rock mass models when β are 90° and 0° increase with joint spacing. Variation curves of equivalent elastic modulus with jointing index are shown in Fig. 15.

It can be noted that the elastic modulus of jointed rock mass specimen decreases rapidly with increasing jointing index m when the loading direction is perpendicular to the joint plane. The decreasing rate of elastic modulus of jointed rock mass specimen when the loading direction is parallel to the joint plane is relatively smaller than that when the loading direction is perpendicular to the joint plane with jointing index. In this figure, it is evident that the variations of equivalent elastic modulus of jointed rock mass models are nonlinear with jointing index m when β are 90° and 0°.

Chen et al. (2014) proposed the same power function as the form of Eq. (11) to analyze the variation curve of equivalent elastic modulus with jointing index:

$$E_{JR}/E_R = c + (1-c)m^{-d} \tag{13}$$

where c and d are the fitting parameters; m is the jointing index.

When using Eq. (12) to analyze the variation curve of equivalent elastic modulus with jointing index, the left side of Eq. (12) needs to be replaced by E_{JR}/E_R.

The results of Eq. (12) in contrast to Eq. (13) are shown in Fig. 16 for analyzing the variation curve of equivalent elastic modulus with jointing index. The parameters of Eqs. (12)–(13) with respect to equivalent elastic modulus and jointing index m of jointed rock mass model and the R^2 and Q are listed in Tables 7 and 8.

Both the fitting curves of Eqs. (12) and (13) agree well with the test data, and the R^2 and Q of Eqs. (12) and (13) match well. Therefore, Eqs. (12) and (13) are applicable to analyze the variation curve of equivalent elastic modulus of jointed rock mass with jointing index.

Discussion

Equation (12) is mainly composed of two power functions and a constant. The fitting curve of Eq. (12) proposed in this study agrees well with the test data when analyzing the variation curve of equivalent peak UCS or equivalent elastic modulus of jointed rock mass with jointing index. However, the fitting accuracy of Eq. (12) may be improved by increasing the

Table 7 Parameters of Eq. (13) when analyzing the variation curve of equivalent elastic modulus with jointing index

β/°	c	d	R^2	Q
0	0.2647	2.15475	0.9971	0.00037
90	0.29313	0.7496	0.9888	0.00075

Table 8 Parameters of Eq. (12) when analyzing the variation curve of equivalent elastic modulus with jointing index

β/°	a	b	c	R^2	Q
0	− 0.9997	1.36637	− 0.09334	0.99847	0.0003
90	− 1.00081	− 0.05994	0.56586	0.98841	0.00117

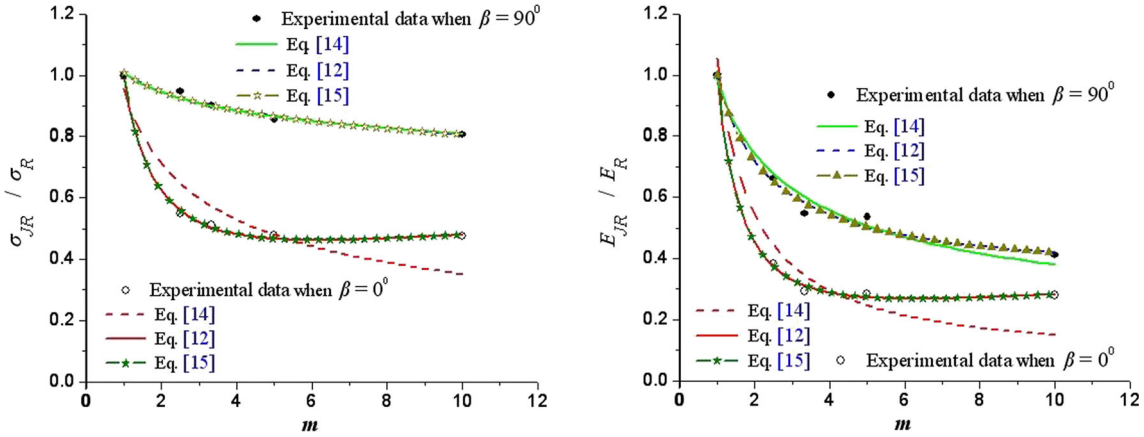

Fig. 17 The fitting curves of Eqs. (12), (14), and (15). Equivalent peak UCS (**a**), equivalent elastic modulus (**b**)

number of power function. Therefore, we expand the number of power function of Eq. (12), i.e., one, two, and three, respectively.

1. When the number of power function is 1, Eq. (12) is changed to be

$$\sigma_{JR}/\sigma_R = a + m^{-b} \tag{14}$$

2. When the number of power function is 3, Eq. (12) is expanded as

$$\sigma_{JR}/\sigma_R = a + m^{-b} + m^{-c} + m^{-d} \tag{15}$$

When using Eqs. (14)–(15) to analyze the variation curve of equivalent elastic modulus with jointing index, the left side of Eqs. (14)–(15) also need to be replaced by E_{JR}/E_R.

The test data shown in Figs. 11 and 14 are analyzed using Eqs. (12), (14), and (15), and the fitting results are shown in Fig. 17. The values of R^2 of Eqs. (12), (14), and (15) are listed in Tables 9 and 10.

Table 9 R^2 of Eqs. (12), (14), and (15) when analyzing the variation curve of equivalent peak UCS with jointing index

β/°	Eq. (14)	Eq. (12)	Eq. (15)
0	0.84583	0.99837	0.99862
90	0.96909	0.97252	0.97341

The R^2 of Eq. (12) is obviously higher than that of Eq. (14), but the R^2 of Eq. (15) is little higher than that of Eq. (12) when analyzing the variation curves of equivalent peak UCS and equivalent elastic modulus with jointing index, when β are 90° and 0°. Therefore, Eq. (12) is appropriate to analyze the variation curves of equivalent peak UCS and equivalent elastic modulus with jointing index. The fitting accuracy of Eq. (12) can be improved by increasing the number of power function. However, the number of power function needs to be determined according to field test results of practical project.

Conclusions

Using the tests on fractured rock mass models in this context, the following conclusions can be drawn:

1. Both the peak UCS and the elastic modulus of jointed rock mass specimen when the loading direction is parallel to the joint plane are greater than those when the loading direction is perpendicular to the joint plane with the same joint connectivity rate and/or the same joint spacing.
2. The difference of peak UCS of jointed rock mass specimen, when β is 90° and 0°, increases with joint connectivity rate. It can be concluded that the anisotropy of UCS

Table 10 R^2 of Eqs. (12), (14), and (15) when analyzing the variation curve of equivalent elastic modulus with jointing index

β/°	Eq. (14)	Eq. (12)	Eq. (15)
0	0.92695	0.99847	0.99848
90	0.97482	0.98841	0.98844

of jointed rock mass tends to increase with joint connectivity rate.

3. The decreasing rates of peak UCS and elastic modulus of jointed rock mass when the loading direction is perpendicular to the joint plane are higher than those when the loading direction is parallel to the joint plane with joint connectivity rate and/or jointing index.
4. The fourth-degree polynomial function proposed in this study is appropriate to analyze the nonlinear variation law of equivalent peak UCS of jointed rock mass with joint connectivity rate. However, the number of times and the number of parameters of multiple polynomial function need to be determined according to lab and field test results of practical projects.
5. The power function proposed in this study is suitable to describe the nonlinear variation laws of equivalent peak UCS and equivalent elastic modulus with jointing index, whilst the number of power function need to be determined according to site-specific test results of practical project.

Funding information This work was financially supported by the Open Research Fund of Key Laboratory of Geotechnical and Underground Engineering of Ministry of Education (Grant No. KLE-TJGE-B1505) and the National Natural Science Foundation of China (Grant Nos. 41541021 and 41230635).

References

Bahaaddini M, Sharrock G, Hebblewhite BK (2013) Numerical investigation of the effect of joint geometrical parameters on the mechanical properties of a non-persistent jointed rock mass under uniaxial compression. Comput Geotech 49:206–225

Bahaaddini M, Hagan P, Mitra R, Hebblewhite BK (2016) Numerical study of the mechanical behavior of nonpersistent jointed tock masses. Int J Geomech 16(1):04015035(1)–04015035(10)

Chen X, Liao ZH, Li DJ (2011) Experimental study of effects of joint inclination angle and connectivity rate on strength and deformation properties of rock masses under uniaxial compression. Chin J Rock Mech Eng 30(4):781–789 [In Chinese]

Chen X, Liao ZH, Peng X (2012) Deformability characteristics of jointed rock masses under uniaxial compression. Int J Min Sci Technol 22: 213–221

Chen X, Liao ZH, Peng X (2013) Cracking process of rock mass models under uniaxial compression. J Cent South Univ 20:1661–1678

Chen X, Li DW, Wang LX, Zhang SF (2014) Experimental study on effect of spacing and inclination angle of joints on strength and deformation properties of rock masses under uniaxial compression. Chin J Geotech Eng 36(12):2236–2245 [In Chinese]

Chen X, Zhang SF, Cheng C (2018) Numerical study on effect of joint strength mobilization on behavior of rock masses with large nonpersistent joints under uniaxial compression. Int J Geomech 18(11): 04018140(1)–04018140(21)

Fan X, Kulatilake PHSW, Chen X, Cao P (2015a) Crack initiation stress and strain of jointed rock containing multi-cracks under uniaxial compressive loading: a particle flow code approach. J Cent South Univ 22:638–645

Fan X, Kulatilake PHSW, Chen X (2015b) Mechanical behavior of rock-like jointed blocks with multi-non-persistent joints under uniaxial loading: a particle mechanics approach. Eng Geol 190:17–32

Goldstein M, Goosev B, Pyrogovsky N (1966) Investigation of mechanical properties of cracked rock. In: Proc. of the 1st Congr. of International Society of Rock Mechanics (Lisbon, Portugal). 1: 521–524

Liu Y, Dai F, Fan PX, Xu NW, Dong L (2017) Experimental investigation of the influence of joint geometric configurations on the mechanical properties of intermittent jointed rock models under cyclic uniaxial compression. Rock Mech Rock Eng 50:1453–1471

Wang LH, Bai JL, Li JL, Tang KY, Deng HF, Sun XS (2011) Study of non-consecutive jointed rock mass under uniaxial compression. ShuiLi XueBao 45(12):1410–1418 [In Chinese]

Yang SQ, Cheng L (2011) Non-stationary and nonlinear visco-elastic shear creep model for shale. Int J Rock Mech Min Sci 48(6): 1011–1020

Yang XX, Qiao WG (2018) Numerical investigation of the shear behavior of granite materials containing discontinuous joints by utilizing the flat-joint model. Comput Geotech 104:69–80

Yang XX, Kulatilake PHSW, Chen X, Jing HW, Yang SQ, Hebblewhite BK (2016) Particle flow modeling of rock blocks with nonpersistent open joints under uniaxial compression. Int J Geomech 16(6): 04016020(1)–04016020(17)

Yang XX, Jing HW, Tang CA, Yang SQ (2017) Effect of parallel joint interaction on mechanical behavior of jointed rock mass models. Int J Rock Mech Min Sci 92:40–53

Zhao WH, Huang RQ, Yan M (2015) Study on the deformation and failure modes of rock mass containing concentrated parallel joints with different spacing and number based on smooth joint model in PFC. Arab J Geosci 8(10):7887–7897